Chinese Chemical Letters 35 (2024) 109037

Contents lists available at ScienceDirect

Chinese Chemical Letters

journal homepage: www.elsevier.com/locate/cclet

Nitric oxide assists nitrogen reduction reaction on 2D MBene: A theoretical study

Chaozheng He[b,c], Jia Wang[c], Ling Fu[d], Wei Wei[a,*]

[a] Henan Engineering Center of New Energy Battery Materials, College of Chemistry and Chemical Engineering, Shangqiu Normal University, Shangqiu 476000, China
[b] School of Chemistry and Chemical Engineering, Shandong Provincial Key Laboratory / Collaborative Innovation Center of Chemical Energy Storage & Novel Cell Technology, Liaocheng University, Liaocheng 252059, China
[c] Institute of Environment and Energy Catalysis, Shaanxi Key Laboratory of Optoelectronic Functional Materials and Devices, School of Materials Science and Chemical Engineering, Xi'an Technological University, Xi'an 710021, China
[d] College of Resources and Environmental Engineering, Tianshui Normal University, Tianshui 741001, China

ARTICLE INFO

Article history:
Received 21 October 2022
Revised 31 August 2023
Accepted 1 September 2023
Available online 4 September 2023

Keywords:
2D mbenes
Nitrogen electro-reduction
DFT
N_2 activation
Ammonia synthesis

ABSTRACT

Electrocatalytic synthesis of ammonia as an environment-friendly and sustainable development method has received widespread attention in recent years. Two-dimensional (2D) materials are a promising catalyst for ammonia synthesis due to their large surface area. In this work, we have constructed a series of 2D metal borides (MBenes) with transition metal (TM) defects (TMd-MBenes) and comprehensively calculated the reactivity of electrocatalytic synthesis of ammonia-based on density functional theory. The results have demonstrated that the TMd-MBenes can effectively activate nitrogen oxide (NO) and nitrogen (N2) molecules thermodynamically. Particularly interesting, the co-chemisorption of O atoms, dissociated from NO, can facilitate the spilled of the inert N2 molecules into single N atoms, which can further hydrogenate into ammonia easily with an ultralow limiting potential of 0.59 V on TMd-MnB. Our research has not only provided clues for catalyst design for experimental study but also paved the way for the industrial application of electrocatalytic ammonia synthesis.

With the development of the human industry and global economy, the energy shortage and environmental pollution have attracted extensive attention [1,2]. Ammonia (NH_3) is one of the most important chemical commodities in human society which is widely applied in the industry [3–6]. NH_3 can be also used as a raw material to synthesis other compounds like fertilizer in agriculture [7–9]. With the development of industrialization, the amount of ammonia produced by human society has increased from 117 million tons in 1996 to 175 million tons in 2016 and the value maintains an increasing tendency [10,11]. Haber-Bosch process is the main method for producing ammonia in the industry which can catalyze the reaction of nitrogen (N_2) and hydrogen (H_2) on iron-based catalysts to generate ammonia. In this process, high temperatures (400–600 °C) and enough pressures (20–40 MPa) are necessary to destroy the highly intensive triple bond (N≡N) [12–14]. However, only 20% efficiency can be achieved for ammonia production at this condition [15]. In addition, some issues on large energy consumption and CO_2 emissions still hinder the development of the industrial synthesis of ammonia. Thus, an eco-friendly method is urgently needed to be developed [5,16-18].

Recently, many fields including electrocatalysis [19–22], photocatalysis [11,23,24], and biological enzyme catalysis are studied in the field of nitrogen reduction reaction (NRR) [25–27]. For electrocatalytic nitrogen reduction to synthesize ammonia, the reduction of N_2 mainly follows associative and dissociative mechanisms. For the associative mechanism, the hydrogen protons and free electrons from an aqueous solution combine with the chemisorbed N_2 on the catalyst [14]. Three different pathways will be followed according to the way of subsequent hydrogenation named distal, alternative, and enzymatic [28]. For dissociated mechanism, the nitrogen molecule will be split into two isolated nitrogen atoms with strong chemisorption on the surface of the catalyst. The following hydrogenation process will be carried out separately on the isolated single nitrogen atoms, which is also the basic principle of the Haber-Bosch process [29]. The mechanism has been investigated comprehensively, while the low activity and selectivity for N_2 reduction still hinder the development of catalysts [30].

Over the past few years, theoretical research has found that the empty d orbitals in the transition metals (TMs, *e.g.*, Fe, Cr, Mo,

* Corresponding author.
E-mail address: weiweizzuli@163.com (W. Wei).

https://doi.org/10.1016/j.cclet.2023.109037
1001-8417/

and V) could receive the long-pair electrons of N_2 molecule, thus separated electrons from TMs would donate to the antibonding orbital [31,32]. N_2 molecules can be effectively activated through this electronic "acceptance-donation" mechanism. Therefore, researchers have tried many new types of electrocatalytic ammonia synthesis materials, including TMs, transition-metal nitrides, carbides, and oxides [33]. On the other hand, the change of catalyst configuration plays a vital role in the improvement of catalytic activity [34], TMs are structured into different structures including single-atom catalysts (SACs) [35–39], vacancy [40–42], core-shell, heterojunction [33], nanoclusters [43], organic framework, and clusters [44]. The non-metal element boron also exhibits an "acceptance-donation" mechanism like TMs in the process of catalyzing N_2 according to the research result of Ling *et al.* [45,46]. Wang *et al.* have also investigated the theoretical mechanism of N_2 reduction from the aspect of carriers recombination [47].

Attributable to special physical and chemical properties, two-dimensional (2D) transition metal borides (MBenes), as an important branch of 2D materials [4,48,49], has been predicted in theory by Sun and coworkers [33] and was experimentally synthesized by Alameda and coworkers in 2018 [50]. MBenes have attracted extensive attention in heterogeneous catalysis due to many characters: metallic properties and numerous elements, which are beneficial to nitrogen activation [51]. Guo *et al.* have conducted a systematic study on 16 different MBenes to synthesize ammonia *via* electrochemical nitrogen reduction reaction (NRR) mode through first-principles calculations [52]. It is identified that CrB, MoB, and WB exhibited intrinsic catalytic activity for NRR with a low limiting potential range of $-0.62 \sim 0.82$ V while could superior suppress the competitive hydrogen evolution reaction (HER). The research results of other scholars on VB, NbB, TiB, *etc*. also show similar properties. However, the position of the boron atom is lower than the transition metal atom, therefore the property of the boron atom could not be displayed during the catalytic process. In addition, most of the research on the electrocatalytic synthesis of ammonia is devoted to the hydrogenation of N_2 molecules to synthesize ammonia according to the associative mechanism [5,53]. Can N≡N bond be broken directly based on the good catalytic activity of MBene?

In this paper, we have constructed the MBenes structure with exposed boron atoms and investigated the possibility of activated N_2 molecules on the transition metal defected MBene (TMd-MBene) surfaces based on density functional theory (DFT) calculation. Referring to our previous research [25], we have considered the synthesis of ammonia with N_2 which can be directly dissociated as the nitrogen source. Herein, we introduced oxygen atoms from NO and investigated whether the presence of O atoms can promote the dissociation of N_2 molecules [54–56], the result showed when O atoms have coexisted on the surfaces of TMd-MBenes, the dissociation procession of N_2 molecules becomes easier, and especially for TMd-CrB and TMd-MoB, the dissociation process of N_2 molecules changes from thermodynamic endothermic to exothermic. Then, the effect of the coexistence of O atoms on the surface of TMd-MBenes on the hydrogenation of N was studied. The free energy diagrams show that the coexistence of oxygen atoms not only reduces the reaction barrier but changes the rate-limiting step of the entire reaction. When NO and N_2 participate in the reaction together, the limiting potential of ammonia synthesis on the surface of TMd-MnB is only 0.59 eV. Finally, a new electrocatalytic reaction mechanism for the synthesis of ammonia from nitrogen molecules is proposed.

VASP (Vienna *Ab initio* Simulation Package) is used in all spin-polarized DFT calculations [57–59]. The projector augmented wave (PAW) method is adopted for the interactions between valence electrons and ion core while the Perdew-Burke-Ernzehof (PBE) functional with the generalized gradient approximation (GGA) was employed to describe the exchange-correlation term [60–62]. A $2 \times 2 \times 1$ supercell of MBene is built which consists of 6 transition atoms and 8 boron atoms with a vacuum space of 20 Å to avoid the interactions between two periodic images [63]. The geometry optimizations and self-consistent calculations are implemented in the cutoff energy of 500 eV and a Monkhorst-Pack k-point mesh of $5 \times 5 \times 1$ is used to sample the Brillouin zone. All the atoms are released until the maximal residual force is less than 0.02 eV/Å during the optimization process. At the same time, the van der Waals (vdW) interactions are described by DFT-D3 [64], and Bader charge analysis evaluated the charge transfer [65]. For electronic structure calculations, we used a $7 \times 7 \times 1$ k-points grid. The projected crystal orbital Hamilton population (pCOHP) was calculated by the LOBSTER code which is used to analyze the chemical bonding between atoms [66].

When we were studying the chemisorption and activation of N_2 molecules and NO molecules on the surface of TMd-MBenes, the chemisorption energy (ΔE_{ads}) of molecules on the surface of the catalysts needs to be considered. This calculation uses the following formula [67,68]:

$$\Delta E_{ads} = E_{tot} - E_{sub} - E_{molecule}$$

where E_{tot} is the total energy of the chemisorbed combination, and E_{sub} and $E_{molecule}$ represent the energy of separate d-MBenes substrate and gas molecules, respectively. It is worth noting that the more negative the value of ΔE_{ads}, the stronger the chemical chemisorption between the gas molecules and the catalysis [69].

The Gibbs free energy change (ΔG) for each elemental step of the ammonia synthesis process is obtained following the computational hydrogen electrode (CHE) model proposed by Nørskov and coworkers [70,71]. The energy of a proton/electron ($H^+ + e^-$) is equal to a half of the chemical potential of hydrogen in this model and the value of ΔG is calculated by the following formula:

$$\Delta G = \Delta E + \Delta ZPE - T\Delta S + \Delta G_{pH} + eU$$

where ΔE is the reaction energy of the product species chemisorbed and reactant on the catalyst surface directedly obtained from DFT calculations; ΔZPE is the zero points and ΔS is the entropies between chemisorbed species and the gas phase molecules, which is calculated from the vibrational frequencies. The reaction temperature and the pH value are set to be 300 K and zero, respectively. ΔG_{pH} is the free energy correction of pH which is calculated by $\Delta G_{pH} = K_B \times pH \times \ln 10$, thus ΔG_{pH} only can be zero in the present research.

The DFT calculation is a commonly used method in catalysis area, which can be combined perfectly with experimental studies. Because it can reveal the geometric and electronic properties from more microscopic level. Ji *et al.* have realized the investigation of bandgap and positions of conduction band/valence band *via* DFT method. These properties are essential for reactivity of catalysis. Thus, DFT method should be widely used in the further studies [72].

The configurations of the 2D material structure of MBene after full geometric optimization are shown in Fig. 1 which is similar to previous research [73]. The 2D material has many merits in the process of catalysis as reported in pioneering works [74,75]. An *et al.* have demonstrated that the 2D borophenes can adsorb ethylene and formaldehyde with forming chemical bonds [74]. MBenes (M denotes Cr, Mn, and Mo) are composed of two layers of transition metal (TM) atoms. In general, TM atoms arrange outmost in MBenes, which can thus be treated as the active sites. To explore the function of the boron atom in the MBenes structures, we have deliberately removed the outmost layer of MBenes as shown in Fig. 1b (this structure is denoted as TMd-MBenes). The position of transition atoms and boron atoms have no change basically except the distance between the top two boron atoms after full opti-

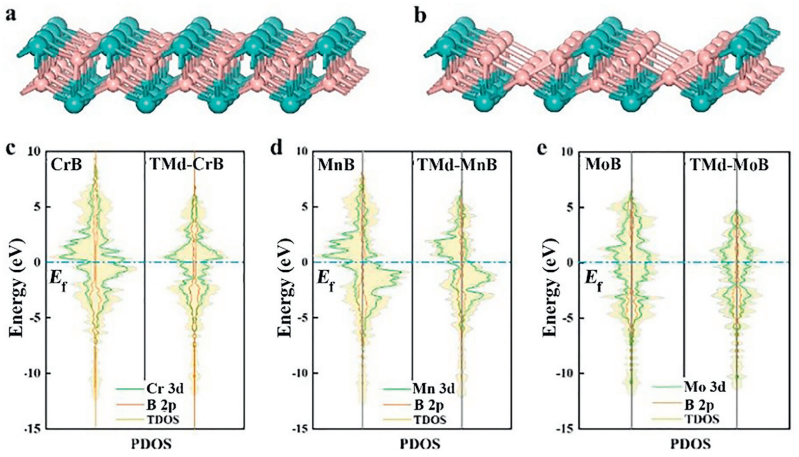

Fig. 1. The schematic configurations of (a) perfect and (b) defective MBene after full geometric optimization. The total and partial density of states (DOS) of (c) CrB and TMd-CrB; (d) MnB and TMd-MnB; and (e) MoB and TMd-MoB. The Fermi level was set to be zero. Dark turquoise and pink spheres represent transition metal atoms and boron atoms, respectively.

mization compared to MBenes (Fig. S1 and Table S1 in Supporting information). All three kinds of TMd-MBenes have been stretched about 0.01–0.02 Å in *b* direction compare to perfect MBenes, the lattice parameter in a direction for TMd-CrB and TMd-MoB have been stretched for −0.02 and 0.01 Å, respectively (Table S1 in Supporting information). These negligible changes of TMd-MBenes indicate that the structure is stable enough for subsequent research on chemisorption and catalytic performance.

The catalysis performance for material is always determined by its electronic properties which should be discussed in-depth. Therefore, we calculated the partial density of states (PDOS) and total density of states (TDOS) for different TMd-MBenes. As shown in Fig. 1c, the TDOS is continuous near the Fermi level for CrB and TMd-CrB which indicates the metallic character. According to the PDOS of Cr-3d and B-2p in a different structure near the Fermi level, the contribution of boron atoms to the metallicity of the TMd-CrB has increased due to the number of Cr atoms decrease. The total magnetic properties of the system come from metal atoms because with the decrease of metal atoms, TMd-CrB shows lower magnetic properties than CrB. The DOS of TMd-MnB and TMd-MoB presented in Figs. 1d and e showed similar characteristics to TMd-CrB. With the increase of magnetic properties, catalytic activity of TMd-CrB improves. As depicted by An *et al.*, the high spin state is beneficial for N_2 adsorption, which can lead to higher reactivity for N_2 reduction [76]. These changes in electronic properties would have an impact on the subsequent chemisorption of gas molecules.

The chemisorption of N_2 and NO on the catalyst surface is the first and most important step in the catalytic reaction to guarantee the activation of inert molecules [77]. Therefore, we first focus our study on the chemisorption behavior of N_2 and NO on the TMd-MBenes surface. As shown in Fig. 2, due to the exposure of boron atoms, there are four different chemisorbed sites on the TMd-MBene surface, named H_B, T_B, H, and T_M, respectively. The chemisorption of N_2 and NO molecules generally includes the vertical and horizontal manners as shown in Fig. 3 with the chemisorption energies for different positions. On the TMd-CrB surface, the maximum chemisorption energy of N_2 on the TMd-CrB surface is −1.39 eV, the maximum chemical chemisorption energies of N_2 molecules on TMd-MnB and TMd-MoB surfaces are −1.75 and −1.25 eV, respectively. In contrast, the chemisorption energy of NO molecule on the TMd-MBenes surface is higher, and the chemisorption energy for the most stable structure is −5.97, −5.91, and −6.25 eV. The T_B and H positions are more favorable for N_2 and NO chemisorption on TMd-MBene except for the situation of TMd-MnB. Since the N_2 molecule includes two perpendicular π bonds and a σ bond, which is far more stable than the NO molecule. Therefore, NO is easily activated, and the corresponding chemisorption energy is also higher compared to N_2. Fig. S2 (Supporting information) shows the lowest energy structure after chemisorption of NO and N_2 molecules. The distance of N atoms in N_2 has stretched into 1.35, 2.90, and 1.4 Å, respectively on TMd-CrB, TMd-MnB, and TMd-MoB. In comparison, The NO molecule is completely dissociated into isolated O and N atoms.

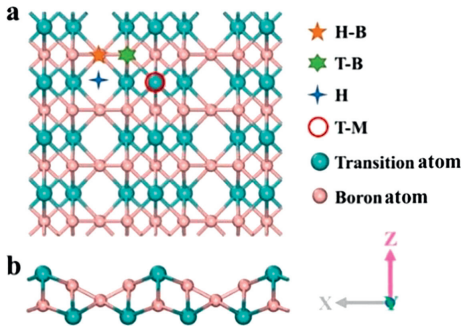

Fig. 2. The (a) top view and (b) side view of adsorption configurations of N2 and NO molecule on TMd-MBenes.

N_2 molecule is different to dissociate due to the strong bond between two nitrogen atoms. Thus the dissociation of the N_2 molecule during the chemisorption process can be treated as a vital step for the subsequent ammonia synthesis, which can be realized on TMd-MBenes. Since NO can dissociate directly on the TMd-MBenes surface, we consider the coexistence of O atoms and N_2 molecules on the TMd-MBenes surface. For the chemisorption on TMd-CrB, N_2 molecule chemisorb on T_B vertically the corresponding chemisorption energy is −1.01 eV and the bond length has been stretched to 1.35 Å, we found the energy of N_2 molecule diffuse to H position is 0.11 eV which is endothermic. As shown in Fig. 4a, when the O atom obtained by the dissociation of NO molecule co-exist on the surface, this process turns into a self-emitting heating procession. For the dissociation of N_2 molecules on the surface of TMd-MnB (Fig. 4b) and TMd-MoB (Fig. 4c), the coexistence of oxygen atoms reduces the thermodynamic dissociation barriers of N_2 molecules by 1.93 and 2.23 eV, respectively. This result indicates that the coexistence of oxygen atoms promotes the reduction of the dissociation energy barrier of N_2 molecules.

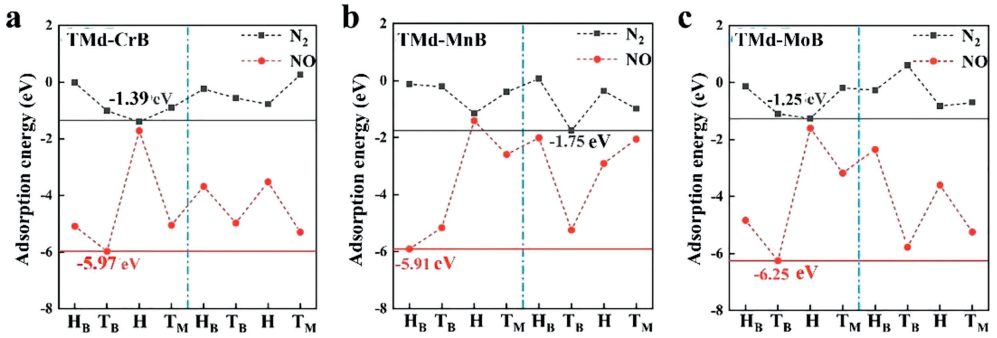

Fig. 3. The chemisorption energy for different positions when N2 and NO molecule chemisorb on the (a) TMd-CrB, (b) TMd-MnB, and (c) TMd-MoB surfaces. The left and right sides of the blue vertical dashed line represent the orientation of molecules placed on the TMd-MBenes surface vertically (left) and horizontally (right), respectively. The dashed lines are added to guide the eye.

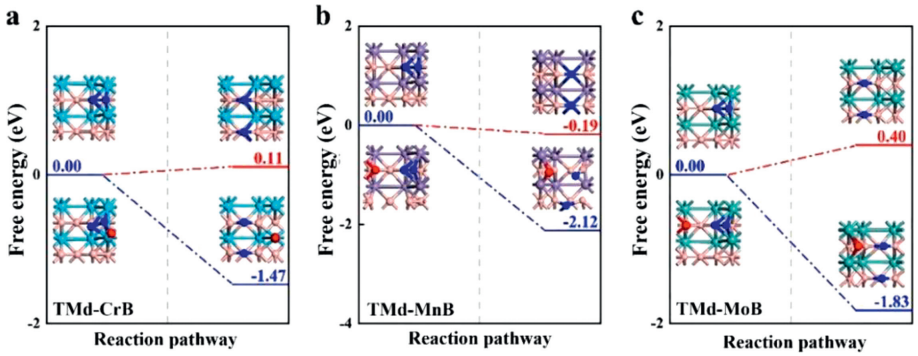

Fig. 4. The free energy change of the N2 dissociation on (a) TMd-CrB, (b) TMd-MnB, and (c) TMd-MoB, respectively. The blue and red lines represent the conditions of oxygen atoms co-adsorption and oxygen-free situation, respectively. The red, blue, and pink spheres represent oxygen, nitrogen, and boron atoms, respectively. The sky blue, purple and dark turquoise spheres of the substrate represent Cr, Mn, and Mo atoms, respectively.

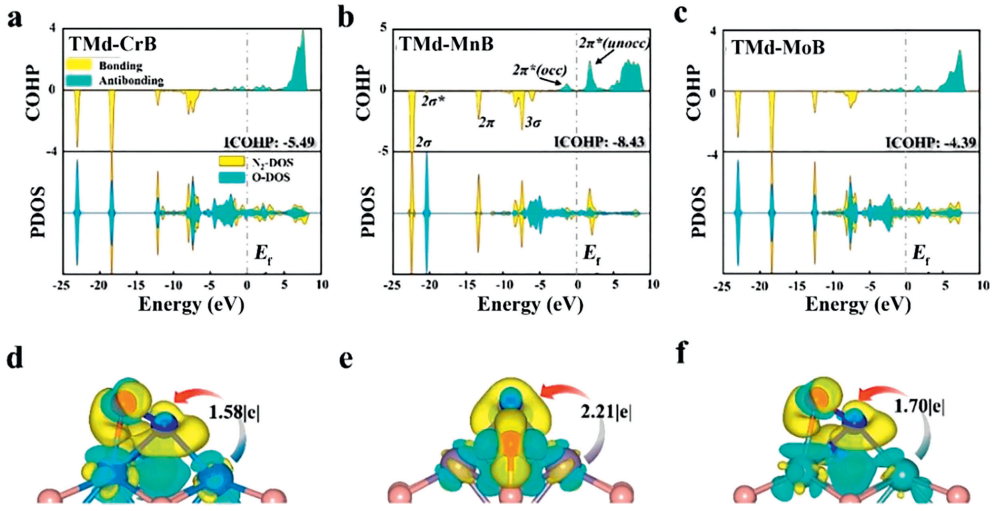

Fig. 5. (a, b, c) The crystal orbital Hamilton populations (COHPs) of N2 on three TMd-MBenes (TMd-CrB, TMd-MnB, and TMd-MoB), respectively, when oxygen atoms coexist and the computed partial density of states (PDOS) of N2 with O atom co-adsorption. The charge density differences and the values of Bader charge transfer for N2 and O atom coexist chemisorption on (d) TMd-CrB, (e) TMd-MnB, and (f) TMd-MoB, respectively. The isosurface value was set to be 0.05 eV/Å3. The red, blue, and pink spheres represent oxygen, nitrogen, and boron atoms, respectively. The sky blue, purple and dark turquoise spheres of the substrate represent Cr, Mn, and Mo atoms, respectively.

To understand the mechanism of N_2 molecular dissociation deeply, we have performed the calculation of electric properties. Fig. 5 shows the crystal orbital Hamilton populations (COHPs) and PDOS of the chemisorbed N_2 molecule and the density of states of the O atom. Compared with the molecular orbitals of free N_2 (Fig. S3 in Supporting information), the electron transfer between N_2 molecules and TMd-MBenes follows the "acceptance-donation" mechanism [78,79]. The N_2 molecules accept electrons from the d orbitals of the transition metals in MBenes, leading to the partial occupation of $2\pi^*$ orbitals near the Fermi level. The COHP also demonstrates that the states of O are hybridized significantly with N_2 with the split of 3σ bonding orbital and the $2\pi^*$ antibonding orbitals for all N_2. By integrating the energy band state to the highest occupied energy level, we obtained the integrated crystal orbital Hamiltonian (ICOHP). The more negative ICOHP corresponds to the stronger coupling between TM-d orbitals and N_2–$2\pi^*$ orbitals. Compared with ICOHP without the participation of O atoms (Fig. S4 in Supporting information), we find that the co-

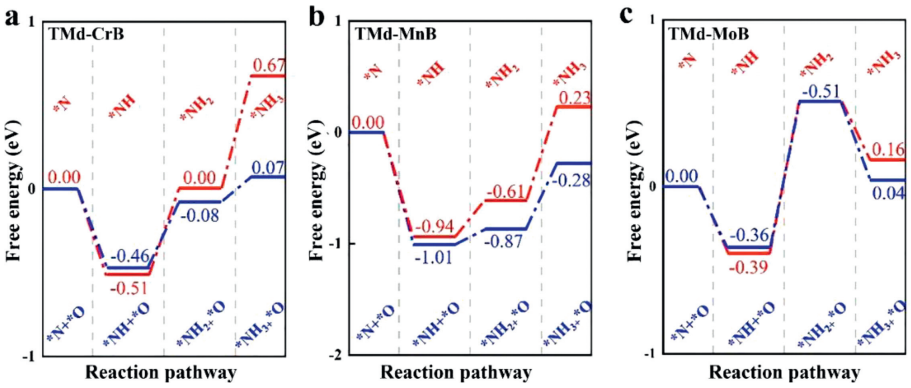

Fig. 6. The free energy diagram for isolated N atom hydrogenation to NH3 (a-c). The Red and blue lines represent the isolated N atom and oxygen atoms coexisting on the surface, respectively.

exist of O atoms enhances the interaction between nitrogen and transition metals. In the case of the coexistence of oxygen atoms, the N_2 molecules ICOHP on the surface of TMd-CrB, TMd-MnB, and TMd-MoB are respectively −5.49, −8.43, and −4.39, which are increased by −0.8, 0.85, and 0.54, respectively compared to the situations without O co-chemisorption. This may stem from the increased charge transfer from the substrate to N_2 under the influence of O atoms (Fig. 5 and Fig. S4 in Supporting information). It is reasonable for one to propose that the co-adsorbed O atom facilitates the interaction between N_2 and the surface, inhibiting its diffusion. Regardless of whether it is bonding or anti-bonding, as well as for the chemisorption and activation of small molecules, MnB is optimal. When calculating the charge difference, it can be seen that the charges transferred from TMd-MBene to N_2 molecule are 1.41, 1.26, and 1.55 |e|, respectively, when the N_2 molecule is chemisorbed. As the O atom adsorbed on the surface, the charge transfer increases significantly especially on TMd-MnB. The charges transferred from the base to the O atom and N_2 molecule are 1.58, 2.21 and 1.70 |e|, respectively.

To further explore the feasibility of synthesizing ammonia on TMd-MBene, we investigate the free energy change of subsequent hydrogenation of N atom to NH_3. The elementary reaction equations can be described as follows:

$$^*N_2 \rightarrow 2^*N \quad (1)$$

$$^*N + H^+ + e^- \rightarrow ^*NH \quad (2)$$

$$^*NH + H^+ + e^- \rightarrow ^*NH_2 \quad (3)$$

$$^*NH_2 + H^+ + e^- \rightarrow ^*NH_3 \quad (4)$$

$$^*NH_3 \rightarrow ^* + NH_3 \quad (5)$$

As shown in Fig. 6a, the reduction of N atom to NH_3 on TMd-CrB generally follows a three-protonation step. The limit step is $^*NH_2 + H^+ + e^- \rightarrow ^*NH_3$ (Eq. 4) in the whole reaction with a limiting potential of 0.67 eV, which can be deduced *via* co-chemisorption of O. Thus, we focus our study on the hydrogenation of N atoms under the coexistence of oxygen atoms (Fig. 6a). After the coexistence of oxygen atoms, the limiting step of N hydrogenate has transformed into $^*NH + H^+ + e^- \rightarrow ^*NH_2$ (Eq. 2) with a deduced limiting energy of 0.38 eV. As O atoms chemisorbed on TMd-CrB, part of the charge on the substrate would be transferred to the oxygen atoms (Table S2 in Supporting information). Compared with the situation without oxygen, the amount of charge distribution on N_xH_y is nearly unchanged.

For the situation of TMd-MnB, $^*NH_2 + H^+ + e^- \rightarrow ^*NH_3$ (Eq. 4) is the limiting step with a reaction energy of 0.84 eV (Fig. 6b). The O co-chemisorption has nearly no influence on reaction energy for ammonia synthesis on TMd-MnB, but the reaction energy barrier has been significantly reduced: The energy barriers of $^*NH + H^+ + e^- \rightarrow ^*NH_2$ (Eq. 2) and $^*NH_2 + H^+ + e^- \rightarrow ^*NH_3$ (Eq. 4) are reduced from 0.33 and 0.84 eV to 0.24 and 0.59 eV, respectively. The presence of oxygen atoms not only reduces the barrier of the rate-limiting step but also makes the remaining hydrogenation steps easier to take place. Table S3 (Supporting information) shows the Bader charge variations of the different moieties in TMd-MnB. When there are O atoms on the surface of TMd-MnB, the amount of charge that N_xH_y obtains from the substrate decreases, and at the same time, a large amount of charge on the substrate is transferred to the oxygen atom.

Finally, we investigated the catalytic procession of TMd-MoB for N atoms and the influence of the presence of oxygen atoms on the reaction procession (Fig. 6c). Regardless of whether there is free oxygen atom chemisorption on the surface of TMd-MoB, the rate-limiting step in the N hydrogenation process is $^*NH + H^+ + e^- \rightarrow ^*NH_2$ (Eq. 3). The coexistence of oxygen atoms only reduces the rate-limiting barrier by 0.03–0.87 eV. At the same time, the exothermic nature of $^*N + H^+ + e^- \rightarrow ^*NH$ (Eq. 2) and $^*NH_2 + H^+ + e^- \rightarrow ^*NH_3$ (Eq. 4) process have not changed. The charge analysis shows that the presence of oxygen atom still has a certain effect on the redistribution of surface charge on TMd-MoB which is shown in Table S4 (Supporting information). The adsorption of N_2 on CrB and MoB are physical sorption and it is chemisorption for MnB. While, the following nitrogen reduction is the protonation process of $^*N$ after $^*N_2$ dissociation, which is independent with the adsorption manner of N_2. Thus, the reaction processes of nitrogen reduction exhibit similar tendencies on MBenes.

In this work, we constructed a defected 2D MBene named TMd-MBene which contains transition atomic defects. We demonstrate using first-principles calculations the defect structure can effectively activate nitrogen molecules and nitric oxide molecules and can dissociate NO molecules. Furthermore, we investigated the influence of oxygen atoms from NO molecules on the activation of N_2 molecules, and the results showed that the dissociation process of N_2 molecules can be thermodynamically transformed from endothermic to exothermic when oxygen atoms coexist. Through the electronic structure analysis of the dissociation process of nitrogen molecules, it is found that the existence of O atoms increases the amount of charge transferred from TMd-MBene to N_2 molecules, which is the reason for coexisting O atoms promoting the dissocia-

tion of N_2 molecules. Finally, we investigated the hydrogenate procession of N atoms on the TMd-MBenes surface to produce ammonia. The free energy diagrams show that the coexistence of oxygen atoms not only reduces the reaction barrier but changes the rate-limiting step of the entire reaction. When NO and N_2 participate in the reaction together, the limiting potential of ammonia synthesis on the surface of TMd-MnB is only 0.59 eV. Our research points out a scheme for activation and dissociation of N_2 molecules, and at the same time, points out new ideas for the experimental electrocatalytic synthesis of ammonia.

Declaration of competing interest

The authors declare that they have no known competing financial interests or personal relationships that could have appeared to influence the work reported in this paper.

Acknowledgments

This study was funded by the Natural Science Foundation of China (No. 21603109), the Henan Joint Fund of the National Natural Science Foundation of China (No. U1404216), the Scientific Research Program Funded by Shaanxi Provincial Education Department (No. 20JK0676), and the Science and Technology Innovation Talents in Universities of Henan Province (No. 22HASTIT028). This work was also supported by Natural Science Basic Research Program of Shanxi (Nos. 2022JQ-108, 2022JQ-096).

Supplementary materials

Supplementary material associated with this article can be found, in the online version, at doi:10.1016/j.cclet.2023.109037.

References

[1] S.W. Gong, G.Q. Zhu, R. Wang, et al., Appl. Catal. B 297 (2021) 120413.
[2] J. Chen, H. Lei, S. Ji, et al., J. Colloid Interface Sci. 601 (2021) 704–713.
[3] C. He, R. Wang, D. Xiang, et al., Appl. Surf. Sci. 509 (2020) 145392.
[4] Y. Wang, M. Batmunkh, H. Mao, et al., Chin. Chem. Lett. 33 (2022) 394–398.
[5] J. Wang, C. He, J. Huo, L. Fu, C. Zhao, Adv. Theory Simul. 4 (2021) 2100003.
[6] L.J. Arachchige, Y. Xu, Z. Dai, et al., J. Mater. Sci. Technol. 77 (2021) 244–251.
[7] L. Gao, F. Wang, M.A. Yu, et al., J. Mater. Chem. A 7 (2019) 19838–19845.
[8] X. Chen, W.J. Ong, X. Zhao, P. Zhang, N. Li, J. Energy Chem. 58 (2021) 577–585.
[9] R. Wang, C. He, W. Chen, et al., Nanoscale 13 (2021) 19247–19254.
[10] S.C. Zhang, D. Chen, Z.F. Liu, M.N. Ruan, Z.A. Guo, Appl. Catal. B 284 (2021) 119686.
[11] C. Liang, W. Cao, L.S. Zhou, et al., ChemCatChem 12 (2020) 1647–1652.
[12] R. Wang, C. He, W. Chen, C. Zhao, J. Huo, Chin. Chem. Lett. 32 (2021) 3821–3824.
[13] S.C. Zhang, B. Zhang, D. Chen, et al., Nano Energy 79 (2021) 105485.
[14] Y. Sun, Y. Wang, H. Li, et al., J. Energy Chem. 62 (2021) 51–70.
[15] Y. Song, X. Li, C. He, Chin. Chem. Lett. 32 (2021) 1106–1110.
[16] J. Yu, C. He, C. Pu, et al., Chin. Chem. Lett. 32 (2021) 3149–3154.
[17] K. Ren, T. Zhang, X. Tan, et al., J. Clean. Prod. 328 (2021) 129658.
[18] Z. Wang, J. Fan, B. Cheng, J. Yu, J. Xu, Mater. Today Phys. 15 (2020) 100279.
[19] L. Fu, R. Wang, C. Zhao, et al., Chem. Eng. J. 414 (2021) 128857.
[20] C. Pu, J. Yu, L. Fu, et al., Chin. Chem. Lett. 32 (2021) 1081–1085.
[21] Y.L. Wu, X. Li, Y.S. Wei, et al., Adv. Mater. 33 (2021) 2006965.
[22] M.A. Hasnat, M.R. Karim, M. Machida, Catal. Commun. 10 (2009) 1975–1979.
[23] H. Lei, M.X. Wu, Y. Liu, et al., Chin. Chem. Lett. 32 (2021) 2317–2321.
[24] L. Wang, G. Huang, L. Zhang, et al., J. Energy Chem. 64 (2022) 85–92.
[25] W. Song, J. Wang, L. Fu, et al., Chin. Chem. Lett. 32 (2021) 3137–3142.
[26] L. Burrows, P.X. Gao, G.M. Bollas, Chem. Eng. J. 426 (2021) 131421.
[27] B.L. Zhang, L.F. Deng, B. Liu, et al., Rare Metals 41 (2022) 166–178.
[28] X. Liang, X. Deng, C. Guo, C.M.L. Wu, Nano Res. 13 (2020) 2925–2932.
[29] L. Cai, N. Zhang, B. Qiu, Y. Chai, ACS Appl. Mater. Interfaces 12 (2020) 20448–20455.
[30] W. Hua, H.H. Sun, F. Xu, J.G. Wang, Rare Metals 39 (2020) 335–351.
[31] Z. Zeng, X. Chen, K. Weng, et al., NPJ Comput. Mater. 7 (2021) 80.
[32] H. Jing, P. Zhu, X. Zheng, et al., Adv. Powder Mater. 1 (2021) 100013.
[33] Y. Sun, Z. Deng, X.M. Song, et al., Nanomicro Lett. 12 (2020) 133.
[34] H. Lei, M.X. Wu, F. Mo, et al., Environ. Sci. Nano 8 (2021) 1398–1407.
[35] G.R. Xu, H. Li, A.S.R. Bati, et al., J. Mater. Chem. A 8 (2020) 15875–15883.
[36] X. Lv, W. Wei, B. Huang, Y. Dai, T. Frauenheim, Nano Lett. 21 (2021) 1871–1878.
[37] H. Zhang, W. Wei, S. Wang, et al., J. Mater. Chem. A 9 (2021) 4082–4090.
[38] S.G. Han, D.D. Ma, Q.L. Zhu, Small Methods 5 (2021) 2100102.
[39] Z. Chen, J.X. Zhao, C.R. Cabrera, Z.F. Chen, Small Methods 3 (2019) 1800368.
[40] H.C. Peng, J. Ren, Y.C. Wang, et al., Nano Energy 88 (2021) 106307.
[41] J.H. Han, S.C. Zhang, Q.G. Song, et al., Sustain. Energy Fuels 5 (2021) 509–517.
[42] P. Chen, Y. Huang, Z. Shi, X. Chen, N. Li, Materials 14 (2021) 2469.
[43] L. Fu, L. Yan, L. Lin, et al., J. Alloys Compd. 875 (2021) 159907.
[44] H. Hu, H. Yang, X. Yang, et al., Chin. Chem. Lett. 31 (2020) 3213–3215.
[45] C. Ling, X. Niu, Q. Li, A. Du, J. Wang, J. Am. Chem. Soc. 140 (2018) 14161–14168.
[46] X. Chen, W.J. Ong, Z. Kong, X. Zhao, N. Li, Sci. Bull. 65 (2020) 45–54.
[47] S. Gao, H.D. Ji, P. Yang, et al., Small 19 (2023) 2206114.
[48] D. Zhou, C. Li, F. Yin, et al., Chin. Chem. Lett. 31 (2020) 2325–2329.
[49] N. Li, J. Peng, W.J. Ong, et al., Matter 4 (2021) 377–407.
[50] L.T. Alameda, P. Moradifar, Z.P. Metzger, N. Alem, R.E. Schaak, J. Am. Chem. Soc. 140 (2018) 8833–8840.
[51] E.M.D. Siriwardane, R.P. Joshi, N. Kumar, D. Cakir, ACS Appl. Mater. Interfaces 12 (2020) 29424–29431.
[52] J. Yang, H. Bai, Y. Guo, et al., Angew. Chem. Int. Ed. 60 (2020) 927–936.
[53] R.Y. Miao, X.X. Li, Q. Lei, et al., Rare Metals 41 (2021) 851–858.
[54] F. Rao, G. Zhu, W. Zhang, et al., ACS Catal. 11 (2021) 7735–7749.
[55] F. Rao, G. Zhu, W. Zhang, et al., Appl. Catal. B 281 (2021) 119481.
[56] Z. Li, Z. Ma, J. Liang, et al., Mater. Today Phys. 22 (2022) 100586.
[57] B. Yang, L.T. Li, Z.Y. Jia, et al., Chin. Chem. Lett. 31 (2020) 2627–2633.
[58] G. Kresse, J. Hafner, Phys. Rev. B: Condense Matter 47 (1993) 558–561.
[59] G. Kresse, D. Joubert, Phys. Rev. B: Condense Matter 59 (1999) 1758–1775.
[60] G. Kresse, J. Furthmüller, Comput. Mater. Sci. 6 (1996) 15–50.
[61] P.E. Blochl, Phys. Rev. B: Condens Matter 50 (1994) 17953–17979.
[62] J.P. Perdew, J.A. Chevary, S.H. Vosko, et al., Phys. Rev. B: Condens Matter 46 (1992) 6671–6687.
[63] C. He, H. Wang, L. Fu, et al., Chin. Chem. Lett. 32 (2021) 990–994 1.
[64] S. Grimme, J. Antony, S. Ehrlich, H. Krieg, J. Chem. Phys. 132 (2010) 154104.
[65] W. Tang, E. Sanville, G. Henkelman, J. Phys.: Condens. Matter 21 (2009) 084204.
[66] R. Dronskowski, P.E. Bloechl, J. Phys. Chem. 97 (1993) 8617–8624.
[67] C. He, R. Wang, H. Yang, S. Li, L. Fu, Appl. Surf. Sci. 507 (2020) 145392.
[68] X. Fu, H. Yang, L. Fu, et al., Chin. Chem. Lett. 32 (2021) 1089–1094.
[69] H. Yang, C. He, L. Fu, et al., Chin. Chem. Lett. 32 (2021) 3202–3206.
[70] J.P. Perdew, Y. Wang, Phys. Rev. B: Condens Matter 45 (1992) 13244–13249.
[71] B. Hammer, J.K. Nørskov, Surf. Sci. 343 (1995) 211–220.
[72] Y. Liu, L. Chen, X.N. Liu, et al., Chin. Chem. Lett. 33 (2022) 1385–1389.
[73] W. Xiong, X.Y. Feng, Y. Xiao, et al., Chem. Eng. J. 446 (2022) 137466.
[74] W.L. Li, Q.G. Jiang, D.D. Li, Z.M. Ao, T.C. An, Chin. Chem. Lett. 32 (2021) 2803-1806.
[75] G.L. Liu, J.H. Zhou, Z.M. Ao, T.C. An, Chin. Chem. Lett. 31 (2020) 1966–1969.
[76] C. Fang, W. An, Nano Res. 14 (2021) 4211–4219.
[77] C. He, J. Wang, L. Fu, C. Zhao, J. Huo, Chin. Chem. Lett. 33 (2022) 1051–1057.
[78] M.A. Legare, G. Belanger-Chabot, R.D. Dewhurst, et al., Science 359 (2018) 896–900.
[79] X.Y. Guo, S.R. Lin, J.X. Gu, et al., Adv. Funct. Mater. 31 (2021) 2008056.